UNIVERSITY OF COPENHAGEN

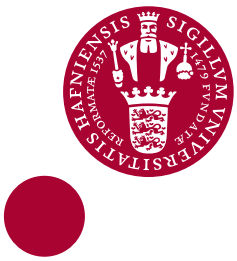

VLT identification of the optical afterglow of the gamma-ray burst GRB 000131 at z=4.50

Andersen, M. I.; Hjorth, J.; Pedersen, H.; Jensen, B. L.; Hunt, L. K.; Gorosabel, J.; Moller, P.; Fynbo, J.; Kippen, R. M.; Thomsen, B.; Olsen, L. F.; Christensen, L.; Vestergaard, Marianne; Masetti, N.; Palazzi, E.; Hurley, K.; Cline, T.; Kaper, L.; Jaunsen, A. O.

Published in:
Astronomy & Astrophysics

Publication date:
2000

Citation for published version (APA):
Andersen, M. I., Hjorth, J., Pedersen, H., Jensen, B. L., Hunt, L. K., Gorosabel, J., ... Jaunsen, A. O. (2000). VLT identification of the optical afterglow of the gamma-ray burst GRB 000131 at z=4.50. *Astronomy & Astrophysics*, *364*, L54-L61.

Download date: 01. Apr. 2020

A&A manuscript no.
(will be inserted by hand later)

Your thesaurus codes are:
13 (13.07.1); 12 (12.03.3); 09 (09.04.1)

ASTRONOMY AND ASTROPHYSICS

arXiv:astro-ph/0010322v1 17 Oct 2000

VLT identification of the optical afterglow of the gamma-ray burst GRB 000131 at $z = 4.50^{\star}$

M.I. Andersen[1], J. Hjorth[2], H. Pedersen[2], B.L. Jensen[2], L.K. Hunt[3], J. Gorosabel[4], P. Møller[5], J. Fynbo[2,5], R. M. Kippen[6], B. Thomsen[7], L.F. Olsen[2], L. Christensen[2], M. Vestergaard[8], N. Masetti[9], E. Palazzi[9], K. Hurley[10], T. Cline[11], L. Kaper[13], and A.O. Jaunsen[14]

[1] Division of Astronomy, University of Oulu P.O. Box 3000, FIN–90014 University of Oulu, Finland
email: Michael.Andersen@oulu.fi
[2] Astronomical Observatory, University of Copenhagen, Juliane Maries Vej 30, DK–2100 Copenhagen Ø, Denmark
[3] Centro per l'Astronomia Infrarossa e lo Studio del Mezzo Interstellare, CNR, Largo E. Fermi 5, 50125 Firenze, Italy
[4] Danish Space Research Institute, Juliane Maries Vej 30, DK–2100 Copenhagen Ø, Denmark
[5] European Southern Observatory, Karl–Schwarzschild–Straße 2, D–85748 Garching, Germany
[6] University of Alabama in Huntsville and NASA/Marshall Space Flight Center, SD50, Huntsville, AL 35812, USA
[7] Institute of Physics and Astronomy, University of Aarhus, DK–8000 Århus C, Denmark
[8] Astronomy Department, Ohio State University, 140 West 18th Avenue, Columbus, OH 43210–1173, USA
[9] Instituto Tecnologie e Studio Radiazoni Extraterresti, CNR, Via Gobetti 101, 40129 Bologna, Italy
[10] University of California, Space Science Laboratory, Berkeley, CA 94720-7450, USA
[11] NASA Goddard Space Flight Center, Greenbelt, MD 20771, USA
[12] Sterrenkundig Instituut "Anton Pannekoek", Kruislaan 403, 1098 SJ Amsterdam, the Netherlands
[13] Institute of Theoretical Astrophysics, University of Oslo, PB 1029, Blindern, N–0315 Oslo, Norway

Received .... ; accepted ....

Abstract. We report the discovery of the gamma-ray burst GRB 000131 and its optical afterglow. The optical identification was made with the VLT 84 hours after the burst following a BATSE detection and an Inter Planetary Network localization. GRB 000131 was a bright, long-duration GRB, with an apparent precursor signal 62 s prior to trigger. The afterglow was detected in ESO VLT, NTT, and DK1.54m follow-up observations. Broad-band and spectroscopic observations of the spectral energy distribution reveals a sharp break at optical wavelengths which is interpreted as a Lyα absorption edge at 6700 Å. This places GRB 000131 at a redshift of 4.500 ± 0.015. The inferred isotropic energy release in gamma rays alone was $\sim 10^{54}$ erg (depending on the assumed cosmology). The rapid power-law decay of the afterglow (index α=2.25, similar to bursts with a prior break in the lightcurve), however, indicates collimated outflow, which relaxes the energy requirements by a factor of < 200. The afterglow of GRB 000131 is the first to be identified with an 8-m class telescope.

Key words: cosmology: observations – gamma rays: bursts – ISM: dust, extinction

1. Introduction

Since the first detections of soft X-ray (Costa et al., 1997), optical (van Paradijs et al., 1997), and radio (Frail and Kulkarni, 1997) afterglows to gamma-ray bursts (GRBs), 19 optical afterglows have been detected.

For the current sample of 12 GRBs with well-determined redshifts, the median redshift is $z_{\rm median}$ = 1.1 with a very large root-mean-square variation of $\sim$0.8. While a photometric redshift of ≈ 5 has been proposed for GRB 980329 (Fruchter, 1999), the highest spectroscopic redshift determination for a GRB so far is $z = 3.418$ for GRB 971214 (Kulkarni et al., 1998). This redshift was determined from the spectrum of a faint Lyman Break galaxy that was found at the position of the optical afterglow (see also Odewahn et al., 1998). The highest redshift determined directly from absorption lines in the spectrum of an optical afterglow is $z = 2.0404 \pm 0.0008$ for GRB 000301C (Smette et al., 2000; Jensen et al., 2000). Several authors have speculated about the possibility of detecting GRBs at even higher redshifts than achieved so far. Wijers et al. (1998) and Lamb & Reichart (2000) estimate that GRBs should be detectable at very high redshifts ($z \gtrsim 5$) based on the assumption that GRBs are associated with star formation and by using models for the cosmic star formation rate as a function of redshift. Blain & Natarajan (2000) propose to use the opposite strategy, namely to use the observed redshift distribution of GRBs to measure the (uncertain) cosmic star formation rate as a function of redshift.

Send offprint requests to: M. I. Andersen

⋆ Based on observations collected at the European Southern Observatory, La Silla and Paranal, Chile (ESO Programmes 64.H-0573, 64.H-0580, 64.O-0187, and 64.H-0313)

Correspondence to: Michael.Andersen@oulu.fi

Table 1. Spectral data from BATSE

Peak Flux:	7.89 ± 0.08 ph cm^{-2} s^{-1} (46–313 keV; 1.024 s)
Fluence:	$(3.51 \pm 0.08) \times 10^{-5}$ erg cm^{-2} (26–1800 keV; 137 s)
Duration:	T90 = 96.3 s (error $\sim$ 1 s)
	T50 = 30.7 s (error $\sim$ 1 s)
Time-averaged	$E_{\rm peak} = 163 \pm 13$ keV
spectral	Low-energy index $= -1.2 \pm 0.1$
parameters:	High-energy index $= -2.4 \pm 0.1$

Unfortunately, afterglows have been detected in only $\lesssim 40$ percent of all well-localized (SAX, RXTE, IPN) GRBs (e.g., Fynbo et al. 2000). It is not clear why most GRBs with no apparent optical afterglow ('dark bursts') are so abundant. Possible explanations are rapid decay (Groot et al., 1998), reddening in the immediate environment and host galaxy (eg., Jensen et al. (2000)), intrinsic optical faintness (Taylor et al., 2000), very high redshifts (Lamb & Reichart, 2000) or a combination of these effects. To shed light on dark bursts, one obvious strategy is to set deeper optical limits by using large telescopes and to determine the decay slopes and colours (see Fynbo et al. 2000).

In this Letter we present the first attempt to identify the afterglow of a GRB with an 8-m class telescope. The attempt was successful in that the observations led to the discovery of the afterglow and the subsequent determination of the decay slope, spectral energy distribution and record high redshift. In the following we document the gamma-ray, optical, and infrared observations, and discuss the properties of the gamma-ray burst and afterglow.

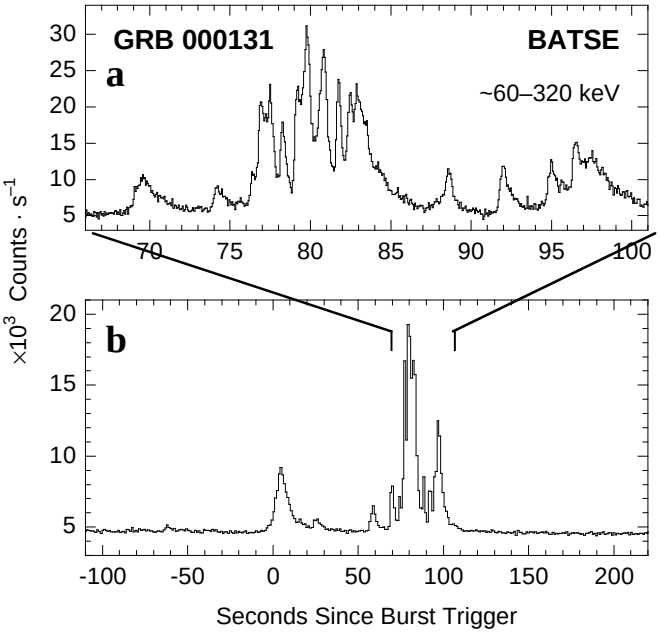

Fig. 1. Gamma-ray light curve of GRB 000131 recorded by the BATSE Large Area Detectors (LADs). **b** shows continuously recorded data with 1024 ms time resolution, **a** shows an enlargement of the most intense interval using triggered data with 64 ms time resolution. In both cases, data from the two most brightly illuminated LADs have been summed. Energy channels for the different data types and detectors have been chosen to approximately match (within a few percent) the energy range 60–320 keV.

2. Detection of the gamma-ray burst

GRB 000131 was observed by Ulysses, Konus/Wind, NEAR, and CGRO-BATSE on 2000 Jan. 31.624 UT. After 56 hours, it was localized via InterPlanetary Network (IPN) timing to two alternate 55 sq. arcmin error boxes (Hurley et al., 2000a), one of which was ruled out by the independent BATSE location (Kippen, 2000). From the Ulysses, Konus/Wind, and NEAR data its 25–100 keV fluence was $\sim 10^{-5}$ erg/cm^2.

BATSE detected the event (Trigger #7975) in a partial data gap, so the standard catalog data products such as flux, fluence, and duration are not available. However, by analyzing other data types from BATSE the relevant parameters could be estimated. The results are given in Table 1. The peak flux is in the top 5%, and the fluence in the top 7% of all BATSE GRBs. The spectrum is well fit by a standard GRB model (Band et al., 1993) and shows a typical spectral evolution (Preece et al., 2000).

The BATSE light curve is shown in Fig. 1. The event consists of several spikes, most of which show a clear asymmetry, the leading edge being the steepest. A weak pulse lasting ≈ 7 s is observed 62 s prior to the burst trigger. Its arrival direction is consistent (within a 12 degree error) with that of the main pulse. This spike is therefore most likely part of the burst. In this case the overall duration is about 170 s, i.e. significantly longer than measured by T90. The presence of this 'precursor' is reminiscent of that displayed by GRB 991216 (Kippen et al., 1999; Hurley, 2000a). However, in the case of GRB 000131, no long-lasting tail (γ-ray afterglow) is observed.

3. Localization and identification of the afterglow

The late localization of the GRB complicated the detection of the optical afterglow, expected to be significantly fainter than the limit of existing sky surveys. Furthermore, the (presumed power-law) decay of the afterglow would be so slow that observations separated by several days would have to be compared before any probable candidate source could be established.

Images of the Inter Planetary Network (IPN) error box were obtained with the FORS1 instrument on Antu (ESO VLT UT1), starting 84 h after the burst. Four 120 s exposures in the B,V and R bands of each of two FORS1 fields, covering the error box (see Fig. 2), were acquired under good seeing conditions (see Table 2 for a log of the observations). On the same night we acquired I–band exposures with a total integration time of 3600 s, using DFOSC on the Danish 1.54-m telescope on La Silla. From this first set of exposures no candidate optical transient could be identified. A subsequent set of images with the same exposure times was acquired 135 h after the burst, under less favorable seeing conditions. Comparing these two epochs, one source located at R.A. = $6^{\rm h}13^{\rm m}31\overset{\rm s}{.}08$, Dec. = $-51^\circ56'41\overset{''}{.}7$

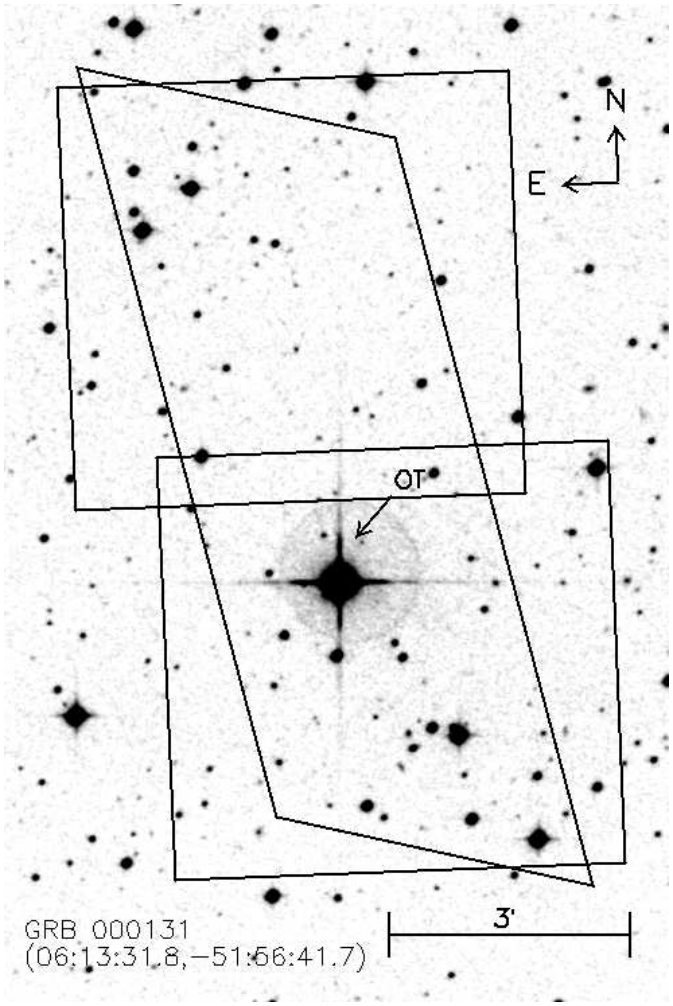

Fig. 2. The rhombus shaped IPN error box with the two square FORS1 fields superimposed. The location of the OT (not present in this Digital Sky Survey image) is marked.

(J2000) was found to have declined by about 1.1 mag in the R–band. In the first epoch images this source was also detected in the V–band, but not in the B–band. Its proximity (1.′1) to the center of the error box, in combination with a fading of about half a magnitude per day, which is typical for GRB afterglows after some days, made this object the likely afterglow of GRB 000131 (Pedersen et al., 2000). The afterglow of GRB 000131 was the second to be identified based solely on an IPN localization (Hurley, 2000a).

4. Follow-up observations and data analysis

Additional images of the field were obtained on 2000 Feb. 8.1 UT. The source was detected in a deep FORS1 R–band exposure and was found to have faded by 1.9±0.2 mag relative to the first epoch confirming its transient nature. As the source, based on the V, R and I photometry, appeared to be very red, we also acquired near-infrared (JHKs) images with the ESO New Technology Telescope (NTT). A final set of R and I band images were acquired with FORS1 on 2000 Mar. 5.0 UT. A log of our photometric observations and the standard calibrated magnitudes of the afterglow is given in Table 2. All image reductions were performed in the IRAF[1] environment.

Table 2. Journal of our observations of GRB 000131.

Telescope	Epoch (2000,UT)	Seeing ($''$)	Band	T_{exp} (sec)	mag
VLT	Feb 4.133	0.9	B	480	>25.85
VLT	Feb 4.135	0.8	V	480	24.66 ±0.10
VLT	Feb 4.137	0.7	R	480	23.26 ±0.04
D1.54	Feb 4.190	1.2	I	3600	22.03 ±0.07
VLT	Feb 6.176	1.3	V	480	>25.40
VLT	Feb 6.183	1.2	R	480	24.35 ±0.14
D1.54	Feb 6.170	1.1	I	3600	>23.70
VLT	Feb 8.091	0.8	R	600	25.13 ±0.19
NTT	Feb 8.046	0.7	J	1680	>22.45
NTT	Feb 8.076	0.7	H	1800	22.25 ±0.30
NTT	Feb 8.103	0.7	Ks	1200	21.47 ±0.41
VLT	Mar 5.025	0.9	R	900	>25.70
VLT	Mar 5.017	1.0	I	900	>24.85

Table 3. Magnitudes of internal reference stars.

Star	B	V	R	I	J	H	K
A	18.97	18.49	18.13	17.77	17.38	17.01	16.88
B	21.60	20.07	18.86	17.48	16.12	15.53	15.25
C	20.79	19.90	19.32	18.86	18.19	17.59	17.53
D	21.15	19.68	18.65	17.67	16.54	15.92	15.73

4.1. Image analysis and photometry

The afterglow was detected at low signal-to-noise in most of the images, which made it essential to use PSF photometry to derive the magnitudes. We used DAOPHOT-II (Stetson, 1987) within IRAF to derive PSF magnitudes of all point sources in the images. In general, when deriving PSF magnitudes, the center and amplitude (magnitude) of the PSF is fitted. For objects close to the detection limit, fitting the centroid introduces a bias in the magnitude of up to one magnitude, because of a tendency to fit the PSF to a nearby noise spike. If instead DAOPHOT is used on objects with accurately known pixel coordinates, the magnitude can be derived without re-centering the object during the PSF fit. In addition to removing the magnitude bias, deriving the PSF magnitude without re-centering also has the advantage that magnitudes down to the 2-σ level can be obtained. We could therefore use the accurate position of the afterglow, as determined from the first epoch images, to derive reliable magnitudes from the observations at later epochs. Limiting magnitudes were obtaind by adding a set of artificial point sources to the images at locations of apparently blank sky, setting the limiting magnitude at the level where DAOPHOT ALLSTAR could recover 95% of the point sources.

[1] IRAF is the Image Analysis and Reduction Facility made available to the astronomical community by the National Optical Astronomy Observatories, which are operated by AURA, Inc., under contract with the U.S. National Science Foundation.

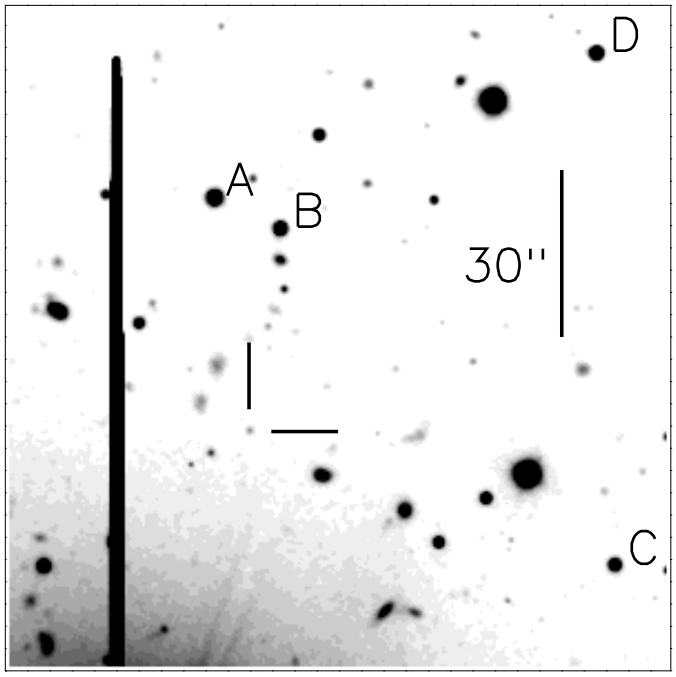

Fig. 3. R–band image of the GRB 000131 afterglow from Feb. 4. The afterglow is marked with two bars and the four comparison stars are labeled according to Table 3. North is up and East is to the left.

4.2. Optical images

The optical observations were all acquired on nights with photometric sky quality. The photometry was calibrated to standard star fields (Landolt, 1992) through CCD aperture photometry relative to the comparison stars marked in Fig. 3 and listed in Table 3. The errors in the magnitudes of the reference stars are dominated by the determination of the photometric zero points. Extinction correction was applied using observatory standard extinction values. Because the standard star exposures were acquired at approximately the same airmass as the object exposures, corrections were in all cases smaller than the individual photometric error of the afterglow magnitude. From the errors in the color transformation, it is estimated that the photometric zero point errors are smaller than 0.02 mag. In the R and I images from Mar. 5, there is no detection of a source within 2″ of the afterglow location. This implies an upper limit to the host galaxy magnitude of R = 25.7 and I = 24.8.

4.3. Near-infrared images

Near-infrared (IR) J, H, and Ks–band images were obtained at La Silla with the NTT and SOFI on 2000 Feb. 8.1 UT. SOFI is equipped with a Hawaii 1024×1024 pixel HgCdTe detector, and we used a plate scale of 0.″29 which gives a field-of-view of roughly 4.′9×4.′9. Each image comprises several tens of elementary co-added frames acquired by randomly dithering the telescope several arcsec once a minute.

The frames were reduced by first subtracting a mean sky, obtained from frames acquired just before and after the source frame. Before using the frames for sky subtraction, stars were eliminated with an automatic star finder coupled with a background interpolation algorithm. Then, a differential dome flatfield correction was applied, and the frames were registered to fractional pixels and combined. We calibrated the photometry with standard stars taken from Persson et al. (1998), acquired directly before and after the source observations. The standards were placed in five different positions on the detector, and reduced in the same way as the source frames. Standard star and source photometry was corrected for atmospheric extinction using the mean ESO La Silla extinction coefficients given in Engels et al. (1981). Formal photometric accuracy, as judged from the standard deviation of the standard star observations, is about 0.03 mag.

At the time of observations, about 8 days after the IPN detection, the afterglow was very faint and thus only marginally detected in H (3 σ) and K (2.5 σ). In J there is apparently a source, but it is displaced about 1 pixel from the location of the afterglow. A PSF magnitude of this source could only be derived if re-centering during the PSF fit was allowed. To maintain consistency in our magnitudes, we have therefore chosen to disregard this apparent source and only give the proper limiting magnitude. The H and K magnitudes are both very close to the detection limit. It was verified that magnitudes at this level can be reliably derived by performing photometry of a large number of artificially added stars of the same magnitude.

4.4. Spectroscopy

Starting 2000 Feb. 8.09 UT, we obtained spectroscopic observations, using FORS1 configured with a 300 lines/mm grism, a cut-on order sorter filter and a 0.″7 slit. The wavelength range covered was 3800 Å – 8200 Å, with a resolution of 9 Å and with order overlap from about 7600 Å. The total integration time was 10800 s, divided into 6 exposures of 1800 s. During the spectroscopic observations, the seeing ranged from 0.″55 to 0.″9. The combined spectrum was flux calibrated relative to the flux standard LTT3218. The continuum is not well detected at visible wavelengths but is weakly detected in the red part of the spectrum, with a signal-to-noise around 1 per spectral bin of 2.5Å in regions that are not dominated by sky lines. The spectral slope is consistent with the broad-band photometry. The spectrum does not show signs of statistically significant emission lines, as could be expected from a host galaxy.

5. Discussion

The temporal and spectral behavior of optical gamma-ray burst afterglows are in general observed to follow a power law, such that $F_\nu(t,\nu) \propto t^{-\alpha}\nu^{-\beta}$ ($\alpha, \beta > 0$), where t is the time elapsed since the GRB event. The fireball model provides the theoretical framework for this behavior and also gives the relation between the temporal slope α and the spectral slope β in various regimes (Sari et al., 1998; Piran, 1999; Meszaros

Table 4. GRB afterglows with rapidly decaying light curves.

GRB	α	β	t_{break}	R(t=4 d)
980326	2.10 $\pm$0.13	0.66 $\pm$0.70		26.4
980519	2.22 $\pm$0.04	0.80 $\pm$0.08	0.55 $\pm$0.17	24.7
990510	2.18 $\pm$0.05	0.61 $\pm$0.12	0.80 $\pm$0.35	22.1
991208	2.20 $\pm$0.20	0.75 $\pm$0.03		20.2
000131	2.25 $\pm$0.19			23.6
000301C	2.29 $\pm$1.00	0.55 $\pm$0.04	4.39 $\pm$1.52	20.6

et al., 1998). If the afterglow is collimated (a jet), the temporal slope is modified and may change during the transition from the observer being inside the jet cone to being outside the jet cone, caused by the slowing-down of the jet (Rhoads, 1999). This results in a break in the light curve, such as those observed in GRB 980519 (Jaunsen et al., 2000), GRB 990123, GRB 990510 (Stanek et al., 1999; Harrison et al., 1999), GRB 990705 (Masetti et al., 2000a), GRB 991216 (Halpern et al., 2000), and GRB 000131C (Jensen et al., 2000; Masetti et al., 2000b). In the following, we will base our discussion on the assumption that the afterglow can be described within the framework of the fireball model.

5.1. The light curve of the afterglow

The three epochs of R–band photometry can be fitted by a power-law decline with $\alpha = 2.25 \pm 0.19$ and a $\chi^2 = 0.06$, as shown in Fig. 4. A power-law decline with this slope is typical for post-break evolution of GRB afterglow emission. A value of $2.0 < \alpha < 2.5$ has been observed in several other afterglows, namely GRB 980326 (Groot et al., 1998), GRB 980519 (Jaunsen et al., 2000), GRB 990510 (Stanek et al., 1999; Harrison et al., 1999; Holland, 2000), GRB 991208 (Hurley et al., 1999; Castro-Tirado et al., 2000), and GRB 000301C (e.g., Jensen et al. 2000). The light curve of GRB 000131 is plotted together with the light curves of these afterglows in Fig. 4. The main characteristics of these systems are summarized in Table 4. In all cases the favoured interpretation of such a steep slope is post-break decay of a collimated outflow. The light-curve breaks predicted in this scenario have indeed been observed (see Holland et al. 2000) and are believed to have occurred prior to the first observations in the other systems with $\alpha > 2$. The simplest interpretation of the GRB 000131 afterglow light curve is therefore that of a collimated outflow seen after the jet has slowed down.

5.2. Spectral energy distribution

The optical afterglow was detected in VRIHK, but at different epochs. By assuming achromatic evolution of the afterglow (which is consistent with other afterglows), following the α = 2.25 power-law decline, the spectral energy distribution can be calculated for a given epoch. In Fig. 5 we plot the derived spectral energy distribution at 3.50 days after the burst trigger, i.e., at the time of the first VRI observations. Also given are the upper limits derived from our B and J observations. The spectral energy distribution has been corrected for Galactic reddening, using $E_{(B-V)}$=0.056 (Schlegel et al., 1998).

For steep-decay afterglows, like those shown in Fig. 4, the large values of α and the relatively small values of β favour a scenario involving a sideways expanding jet. In this case spec-

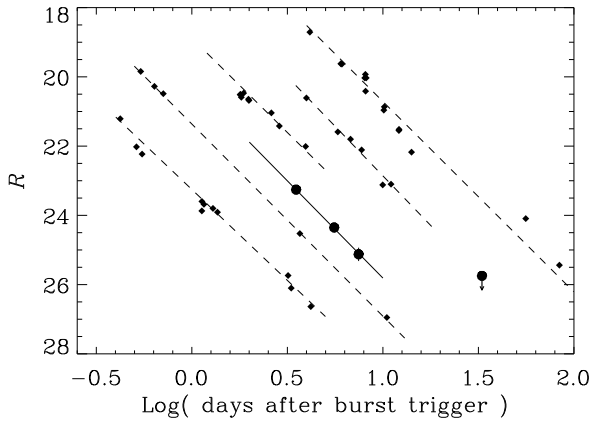

Fig. 4. R–band light curves of GRB afterglows with steep late-time decay. The solid line is a power-law fit to the GRB 000131 data (filled circles). The non-detection on March 5 is marked as an upper limit at $\log t$=1.52. Other afterglows are (from left to right) GRB 980326, GRB 980519, GRB 990510, GRB 000301C and GRB 991208 (which is shifted 0.4 in log(days)). Pre-break data points are omitted.

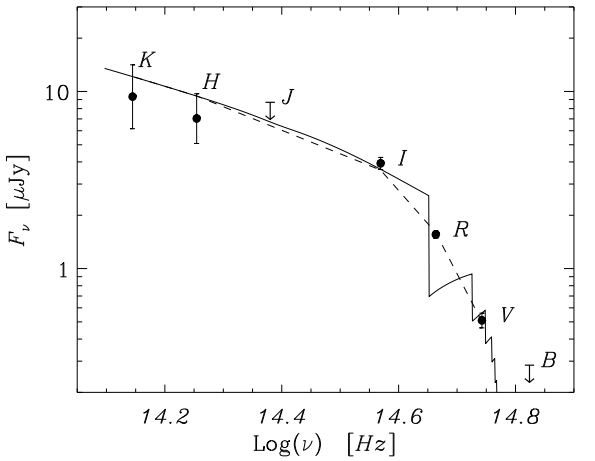

Fig. 5. The spectral energy distribution, as derived from broad band photometry. The errors of the H and K fluxes include the formal error from the extrapolation of the light curve back to t=3.5 days. A fit by a power law spectrum with Lyman forest absorption and SMC reddening is shown as a dashed line. This yields A_V = 0.18, when an intrinsic spectral slope, β = 0.70, and a redshift of 4.5 is assumed. The solid line shows the corresponding spectrum with its Lyman absorption edges.

tral slopes between $(\alpha - 1)/2$ and $\alpha/2$ are expected in the fireball model, depending on the value of the cooling frequency. With $\alpha = 2.25$, this implies $0.63 < \beta < 1.13$, with a preference for the low value (cf. Table 4).

The spectral energy distribution shown in Fig. 5 does not resemble a power-law with a single index β. This is not an artifact of extrapolating the H and K band data points from Feb. 8 to Feb. 4, as a power-law fit to the V, R, and I data points only results in a $\chi^2 = 7.1$ and $\beta = 4.90$, which is much steeper than the value of about 1 typically observed in GRB afterglows (see Table 4). Moreover, for the H and K fluxes to be in accordance with this fit, an unphysical value of α of about 7.0 in the near-IR is required. Thus, a power-law spectral energy distribution is ruled out.

We have explored whether the strongly curved shape of the spectral energy distribution can be explained by reddening in the host galaxy (as in eg. GRB 000301C, Jensen et al. 2000, or in GRB 971214, Dal Fiume et al. 2000). We find that no physically plausible reddening laws can transform a power-law spectrum into the observed shape.

The most likely interpretation of the spectral break is therefore the onset of Lyman forest blanketing, hence implying that GRB 000131 was at a high redshift (z$\gtrsim$4). To examine this interpretation further we have fitted the spectral energy distribution with power-laws modified by the effects of Lyman forest blanketing and internal reddening in the host galaxy. This technique was first used by Fruchter (1999) for GRB 980329 and discussed in detail by Reichart (2000). For the reddening we use the SMC extinction law assumed to best represent a chemically less-evolved environment at redshifts of 4 to 5. To model the effects of Lyman forest blanketing we follow Møller and Jakobsen (1990): for each pair of values of β and z, the visual rest-frame absorption A_V and the χ^2 of the fit is obtained. We find that all values of β allowed by the fireball model are possible, with a preference for low values. The corresponding range of internal reddening is $0.11 < A_V < 0.20$, with a preference for high values. For values of β around 0.65, the possible range (2 σ) of redshifts is $4.38 < z < 4.70$, while the redshift is $4.55 < z < 4.69$ for β = 1.0. This result is not affected by the choice of reddening law.

5.3. The spectroscopic redshift of GRB 000131

Our analysis of the photometric observations implies the presence of a Lyα absorption edge in the range 6500 Å to 6900 Å. This implication is confirmed by the spectroscopic observations. After smoothing the FORS1 spectrum to a resolution of 30 Å a clear indication of such an absorption edge at 6700 Å is revealed. The recorded spectrum was very faint, at the level of less than 2% of the continuum of the night sky, which is dominated by emission lines through the red part of the spectrum. The noise in the spectrum is therefore dominated by uncertainty in the sky subtraction. An improved representation of the continuum was obtained by rebinning the spectrum to a resolution of 200 Å, omitting spectral bins coincident with sky lines. The smoothed and the rebinned spectra are shown in Fig. 6 together with a model of the spectrum, assuming a redshift of 4.5, β = 0.70 and a reddening, $A_V = 0.18$, as derived from a fit to the photometry (see Fig. 5).

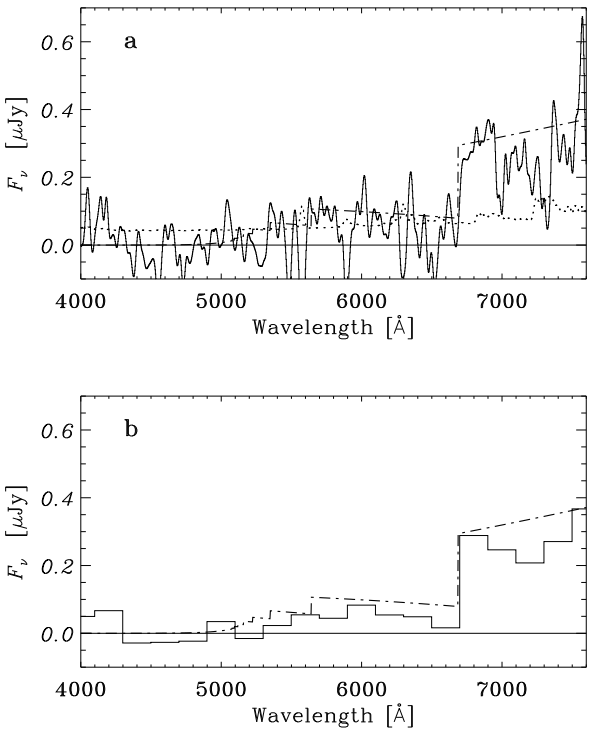

Fig. 6. The spectrum of the GRB 000131 afterglow: **a** smoothed to a resolution of 30 Å, **b** rebinned to a resolution of 200 Å. The dotted curve shows the noise per bin, while the dot-dashed line is the model spectrum shown in Fig. 5.

The model spectrum is normalized to the R-magnitude of the afterglow, obtained immediately before the spectroscopic observations began, and corrected for slit losses of 35%, as would result from using a 0.″7 slit in a seeing of about 0.″7. The model spectrum is seen to be in very good agreement with the binned spectrum for wavelengths below 7200 Å. The average observed flux in the Lyman forest region (between Lyα and Lyβ) is 55 ± 15 nJy, which is in reasonable agreement with the level of 79 nJy predicted by the model. Beyond 7200 Å the spectrum is dominated by an atmospheric band and strong sky lines, which are not well resolved at a spectral resolution of 9 Å. This effectively renders the spectrum useless in this spectral region.

As the spectral region from 6590 Å to 6810 Å is essentially free from sky lines, the location of the absorption edge is well defined (see Fig. 7). We measure its location to be at 6701 ± 2.5 Å from which a redshift of 4.511 ± 0.002 is inferred. The reality of the absorption edge and the interpretation that it is due to Lyα is most convincingly seen by integrating the flux of the spectrum and the model, as shown in Fig. 7. The integrated spectrum is very smooth and follows the model nicely on the red side of the edge, while there are significant

deviations on the blue side of the edge. Comparing 100 Å intervals on the blue and red side of the absorption edge, the standard deviation of the spectrum is found to be 65% larger on the blue side, consistent with the interpretation that the blue side is located in the Lyman forest. Hence, the VLT spectrum is in excellent agreement with the photometric observations and provides independent evidence that the redshift of GRB 000131 is $z \approx 4.5$.

In the VLT spectrum of GRB 000301C, Jensen et al. (2000) detected a strong damped Lyα absorption line at the redshift of the GRB. If a similar damped Lyα absorption line is present in the spectrum of GRB 000131 the redshift as determined from the spectral break will be slightly overestimated since the red wing of the damping profile will move the spectral break 10–20 Å (depending on the H I column density) towards the red. Therefore, the inferred redshift from the spectral break depends on the assumed H I column density of the GRB self absorption. With the signal-to-noise of the spectrum, it is not possible to constrain the H I column density. An indirect indication that GRB 000131 had significant self absorption is obtained from the estimate of A_V. Assuming an SMC extinction law and minimum dust-to-gas ratio (Pei, 1992) and the maximum value of A_V, as derived from the fit of the spectral energy distribution, an H I column density of up to 10^{22} cm^{-2} is estimated. An estimate of the likely error of the redshift may therefore be obtained by fitting a H I line corresponding to this column density to the spectrum. We derive a redshift of 4.490 $\pm$0.002 for this column density, which allows us to conservatively conclude that the redshift of GRB 000131 is $z = 4.500 \pm 0.015$.

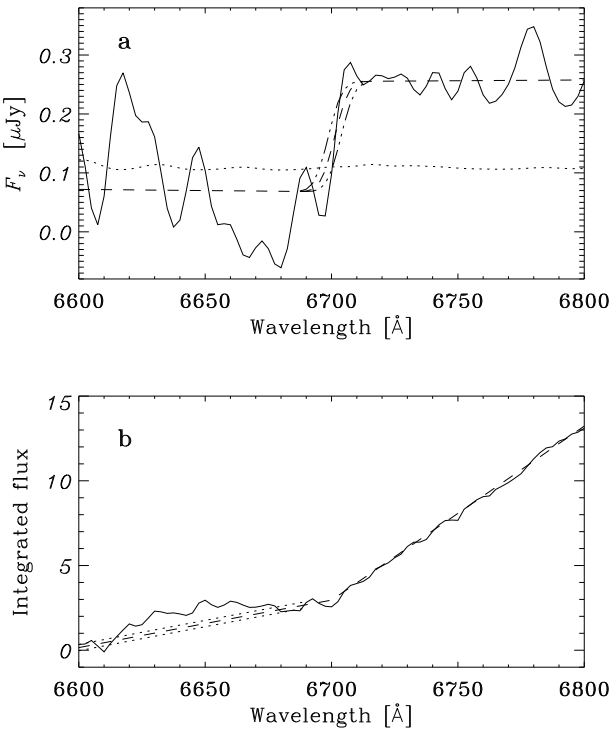

Fig. 7. a A region of the spectrum, centered on the Lyα absorption edge and smoothed to a resolution of 13 Å. The dotted line gives the noise per bin, while the dashed curve is a model absorption edge spectrum corresponding to a redshift of 4.511, and redshifts of 4.509 and 4.513 (dot-dashed curves). **b** The integrated flux of the full resolution spectrum and the model absorption edge spectra shown in **a**. The integrated flux is normalized to a common level at 6750 Å .

6. Conclusions

Based on the temporal and positional coincidence of the transient object with GRB 000131, and the fact that it was located at a cosmological distance, we conclude that this transient object was the optical afterglow of GRB 000131. Assuming a Hubble constant of 65 km s^{-1} Mpc^{-1}, $\Omega_0 = 0.3$ and $\Omega_\Lambda = 0.7$, a redshift of 4.50 implies a distance modulus of 48.24. Hence, the total energy release assuming isotropic emission is $\approx 1.1 \times 10^{54}$ erg. This is only a factor of $\sim$3 smaller than the isotropic equivalent energy for the most energetic event so far, GRB 990123 (Andersen et al., 1999; Kulkarni et al., 1999). However, the combination of the decay slope α and the constraints on the spectral slope β indicate that the afterglow was due to a collimated jet. The upper limit on the break epoch, $t_{\rm break} < 3.5$ days, implies a lower limit on the jet opening angle of $\theta > 7^\circ\ n^{1/8} > 7^\circ$, where n is the density of the ambient medium (in units of cm^{-3}), which is larger than 1 in star-forming regions. From the lower limit on the opening angle we infer a lower limit on the released energy of $\sim 5 \times 10^{51}$ erg.

This work shows that 8-m class telescopes may be used successfully to detect faint R > 23 optical afterglows even in fields with very bright stars. This is necessary in order to resolve why $\gtrsim 60\%$ of all attempts to detect optical afterglows of GRBs are currently unsuccessful (Fynbo et al., 2000). The apparent brightness of the GRB 000131 afterglow was similar to that of GRB 990123. GRB 000131 does therefore provide the first observational evidence that it is possible to obtain high resolution optical spectra of GRBs at very high redshift, if the afterglow is identified at an early time. High redshift GRBs will therefore no doubt prove to be an extremely valuable tool for not only the understanding of the GRB environment but also for the study of the Lyman forest and of cosmology.

Acknowledgements

MA acknowledges the Astrophysics group of the Physics dept. of University of Oulu for support of his work. This work was supported by the Danish Natural Science Research Council (SNF). Part of the data presented here were obtained as part of an ESO Service Mode programme. The allocation of observing time by IJAF at the Danish 1.54 m telescope on La Silla is acknowledged. KH is grateful for support under JPL Contract 958056 for Ulysses operations, and to NASA Grant NAG 5 9503 for NEAR operations. We are grateful to the NEAR XGRS team and the Konus/Wind team for the use of their data in localizing this burst. MV gratefully acknowledges financial

support from the Columbus Fellowship at The Ohio State University.

References

Andersen, M. I., Castro-Tirado, A. J., Hjorth, J., et al., 1999, Science 283, 2075
Band, D., Matteson, J., Ford, L., et al., 1993, ApJ 413, 281
Blain, A. W. and Natarajan, P., 2000, MNRAS 312, L35
Castro-Tirado, A.J., Sokolov, V. V., Gorosabel, J. et al., 2000, A&A in preparation
Costa, E., Frontera, F., Heise, J., et al., 1997, Nature 387, 783
Dal Fiume, D., Amati, L., Antonelli, L.A. et al., 2000, A&A 355, 454
Engels, D., Sherwood, W. A., Wamsteker, W., and Schultz, G. V., 1981, A&AS 45, 5
Frail, D. A. and Kulkarni, S. R., 1997, IAU Circular 6662
Fruchter, A. S., 1999, ApJL 512, L1
Fynbo, J. U., Jensen, B., Gorosabel, J., et al., 2000, A&A submitted
Groot, P. J., Galama, T. J., Vreeswijk, P. M., et al., 1998, ApJ 502, L123
Halpern, J., Uglesich, R., Mirabel, N., et al., 2000, ApJ astro-ph/0006206, in press
Harrison, F. A., Bloom, J. S., Frail, D. A., et al., 1999, ApJ 523, L121
Holland, S., Björnsson, G., Hjorth, J., Thomsen, B., 2000, A&A submitted
Hurley, K., Cline, T., 1999, GCN circular No. 450
Hurley, K., Cline, T., Mazets, E., et al., 2000, ApJL 534, L23
Hurley, K., Cline, T., Mazets, E., 2000, GCN circular No. 529
Jaunsen, A., Hjorth, J., Björnsson, G., et al., 2000, ApJ in press
Jensen, B. L., Fynbo, J., Gorosabel, J., et al., 2000, A&A submitted
Kippen, R. M., Preece, R. D., Giblin, T., 1999, GCN circular No. 463
Kippen, R. M., 2000, GCN circular No. 530
Kulkarni, S. R., Djorgoski, S. G., Ramaprakash, et al., 1998, Nature 393, 35
Kulkarni, S. R., Djorgovski, S. G., Odewahn, S. C. et al., 1999, Nature 398, 389
Lamb, D. Q., Reichart, D. E., 2000, ApJ 536, 1
Landolt, A. U., 1992, AJ 104, 340
Masetti, N., Palazzi, E., Pian, E., et al., 2000, A&A 354, 473
Masetti, N., Bartolini, C., Bernabei, S., et al., 2000, A&A 359, L23
Meszaros, P., Rees, M. J., Wijers, R. A. M. J., 1998, ApJ 499, 301
Møller, P., Jakobsen, P., 1990, A&A 228, 299
Odewahn, S. C., Djorgovski, S. G., Kulkarni, et al., 1998, ApJ 509, L5
Pedersen, H., Jensen, B., Hjorth, J., et al., 2000, GCN circular No. 534
Pei, Y. C., 1992, ApJ 395, 130
Persson, S. E., Murphy, D. C., Krzeminski, W., Roth, M., Rieke, M. J., 1998, AJ 116, 2475
Piran, T., 1999, Phys Rep 314, 575
Preece, R. D., Briggs, M. S., Mallozzi, et al., 2000, ApJS 126, 19
Reichart, D. E., 2000, ApJ submitted
Rhoads, J. E., 1999, ApJ 525, 737
Sari, R., Piran, T., Narayan, R., 1998, ApJ 497, L17
Schlegel, D. J., Finkbeiner, D. P., Davis, M., 1998, ApJ 500, 525
Smette, A., Fruchter, A. S., Gull, T. R. et al., 2000, ApJ submitted
Stanek, K. Z., Garnavich, P. M., Kaluzny, J., Pych, W., Thompson, I., 1999, ApJ 522, L39
Stetson, P. B., 1987, PASP 99, 191
Taylor, G. B., Bloom, J. S., Frail, D. A., et al., 2000, ApJL 537, L17
van Paradijs, J., Groot, P. J., Galama, T., et al., 1997, Nature 386, 686
Wijers, R. A. M. J., Bloom, J. S., Bagla, J. S., Natarajan, P., 1998, MNRAS 294, L13